Two-Dimensional Condensation of Guanidinium Nitrate at the Mercury–Water Interface

Thomas Wandlowski, Geoffrey B. Jameson, and Robert de Levie*

Department of Chemistry, Georgetown University, Washington, D.C. 20057

*Received: April 1, 1993; In Final Form: June 9, 1993**

Guanidinium cations can form a condensed interfacial monolayer with nitrate anions, in which the two ions participate in a one-to-one ratio. The earlier results of Dyatkina et al. (*Elektrokhimiya* **1980**, *16*, 996) have been confirmed and extended. The formation of the monolayer film is controlled by the kinetics of nucleation and two-dimensional growth. Most likely, the film is held together by multiple hydrogen bonds between the nitrate oxygens and the amine hydrogens of the guanidinium ions, in an interfacial organization similar to that in the layered crystal structure reported here.

Introduction

The properties of compact monolayer films made by two-dimensional condensation of molecules adsorbed at the mercury–water interface have been studied extensively during the past decade and have been reviewed several times.[1-4] Less well-studied are condensed monolayer films made from adsorbed salts, even though they have been known almost as long[5] as their neutral counterparts.[6] In a recent series of papers[7-9] we have reported on the properties of films made by tetrabutylammonium salts. In that case, compact films were observed in the presence of all anions investigated: F^-, Cl^-, Br^-, I^-, SCN^-, ClO^-, and SO_4^{2-}.

In the present communication, we will focus on the formation of a compact film containing guanidinium cations, which is much more selective, in that two-dimensional condensation is mostly restricted to the presence of nitrate counterions. This system was first studied by Dyatkina et al.[10] Other studies involving the adsorption of guanidinium ions at the mercury–water interface have found no evidence of film condensation in the presence of chloride[11] or perchlorate anions.[12]

Dyatkina et al.[10] reported both capacitance and interfacial tension measurements. The latter yielded a value of 2.9 μmol m^{-2} for the interfacial excess of guanidinium nitrate in the condensed film, corresponding with an area of 0.57 nm^2 per guanidinium–nitrate pair, a value they interpreted as due to a monolayer of dehydrated guanidinium and nitration ions. In this article we will first describe some thermodynamic properties of the condensed film formed by guanidinium nitrate. We will show that such a film indeed contains equal numbers of cations and anions and that film condensation therefore can be described in terms of an interfacial analogue of a solubility product. We will then show that the stability of this film can be understood in terms of a modified statistical-mechanical model used for two-dimensional films composed of neutral molecules. We also report the crystal structure of guanidinium nitrate, which supports the electrochemical conclusions regarding the molecular composition of the film. We then shift our focus toward the kinetic mechanisms involved in the formation and dissolution of those interfacial structures and end with a brief discussion of the properties of this film towards electrode reactions.

Experimental Methods

All capacitance measurements were made using a hanging mercury electrode of 2.37_5 mm^2 area, formed at the end of an unsiliconized glass capillary in a PAR 303 mercury dispenser. A platinum wire was used as auxiliary electrode and an external saturated calomel electrode, maintained at room temperature, as the reference electrode. All potentials given are referred to this electrode and were reproducible to within ±0.2 mV. The cell temperature was controlled to within ±0.2 °C. Unless otherwise stated, it was kept at +5.0 °C.

The capacitance was measured by superimposing a 1.59-kHz sine wave of 2.5-mV amplitude on a voltage step or voltage ramp. In the latter case, the absolute value of the scan rate was 5 mV s^{-1}. Maximum iR compensation short of oscillations was used to reduce the uncompensated solution resistance. The cell current was converted into a voltage, and its ac component amplified, synchronously rectified with a lock-in amplifier, digitized, and stored in an AT-type computer for subsequent data processing. Further experimental details are as described elsewhere.[13]

All solutions were made from pyrodistilled water and Merck Suprapur chemicals. Moreover, all supporting electrolyte solutions were treated with activated charcoal before use. Guanidinium nitrate and guanidinium fluoride were prepared by quantitative precipitation of guanidinium chloride with silver nitrate and silver fluoride respectively.

For the determination of the crystal structure of guanidinium nitrate, crystals were grown by slow evaporation of a solution of the salt in a water–methanol mixture. Most of the resulting crystals were unsuitable for single-crystal analysis. Eventually one marginally suitable crystal was found. The nonstandard setting $I2/m$ of the standard setting of the space group $C2/m$ was chosen as the cell is nearly orthogonal. The underlying primitive cell is pseudorhombohedral (a = 743.1 pm, b = 743.4 pm, c = 750.2 pm, α = 58.33°, β = 58.31°, γ = 58.98°), whence in part the difficulties in finding a suitable single crystal.

Toward the end of the crystal structure analysis it became apparent from unrealistic bond distances calculated for guanidinium and nitrate ions and from the location of residual electron density around the nitrate ion, that models involving disorder of the sites assigned to guanidinium and nitrate ions should be investigated. Highly restrained refinements based on the near-superposition of a nitrate ion (with an N–O distance of 124.2 pm) on a guanidinium ion (with a C–N distance of 132.4 pm) were unstable but did lead to a substantial improvement in the agreement between the observed and calculated structure factors, F_o and F_c. Satisfactory convergence was finally achieved for a cruder model that assumed exact superposition of nitrate and guanidinium ions. This led to a final difference Fourier map that was flat and featureless. A calculated relative site occupancy of 0.51 ± 0.04 corresponds to a total absence of registry between adjacent layers of guanidinium nitrate ions since, within a layer, direct cation–cation and anion–anion contacts are not likely. The final C–N and N–O distances are equal within the experimental uncertainty (see Table IV) and are close to the simple average of (128.2 ± 0.3 pm) of these distances in the precise redetermination[14] of the crystal structure[15] of methylguanidinium nitrate. These features are consistent with the scrambling of nitrate and

* Abstract published in *Advance ACS Abstracts*, September 1, 1993.

0022-3654/93/2097-10119$04.00/0

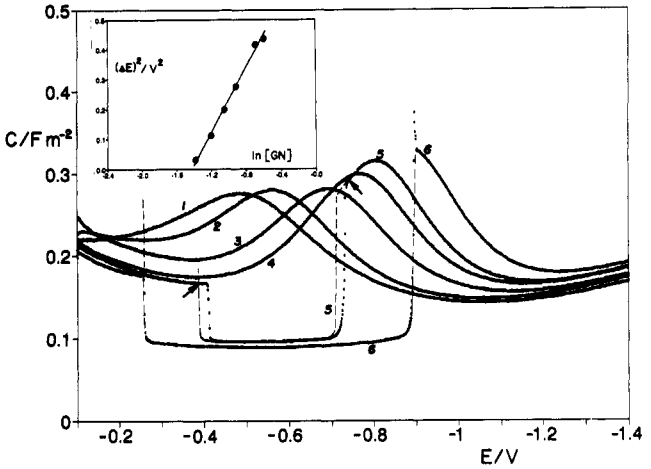

Figure 1. Interfacial capacitance C of mercury in contact with aqueous solutions of guanidinium nitrate as a function of the applied potential E vs SCE. Guanidinium nitrate concentrations: (1) 0.025; (2) 0.050; (3) 0.10; (4) 0.20; (5) 0.30; (6) 0.50 M. Temperature 5 °C, measuring frequency 1.59 kHz, amplitude 2.5 mV, voltage scan rate −5 mV s^{-1}. For curve 5, the reverse scan, with a scan rate of +5 mV s^{-1}, is also sketched in, with a thin broken line. At the highest concentration used, the hysteresis is negligible, see curve 6. Arrows on curve 5 identify the points used to determine the pit width ΔE. The inset shows the dependence of $(\Delta E)^2$ on the natural logarithm of the guanidinium nitrate concentration [GN]. The solid line represents a least-squares line through these points, of which the parameters are listed in Table I.

guanidinium sites in the asymmetric unit. The improvement in the weighted R index (as defined in Table II), based on F^2 of all data ranged from 0.266 to 0.198 for the addition of a parameter specifying the relative amounts of guanidinium (including hydrogen atoms) and nitrate. The corresponding improvement in the more conventionally quoted R index on F, for data with $F > 4\sigma(F_o)$, ranged from 0.085 to 0.071. The crystallographic mirror plane bisects an O–N–O bond angle and C–N–C bond angle.

Capacitance as a Function of Potential and Concentration

Figure 1 illustrates the dependence of the differential capacitance of the mercury–solution interface on the aqueous concentration of guanidinium nitrate and on potential, in the absence of any other electrolyte. The morphology of curves 1–4 is comparable to those obtained for guanidinium perchlorate[12] and sodium nitrate[16] at similar concentrations. At the two highest guanidinium nitrate concentrations shown, the curves exhibit regions of potential with an abruptly lower interfacial capacitance, the so-called capacitance pits, which are the focus of this paper.

In such capacitance pits, a monolayer is believed to be present at the mercury–solution interface, and the rate of formation of such a monolayer is often controlled by the kinetics of nucleation and two-dimensional growth characteristic of a phase transition.[1-4] Curve 5 of Figure 1 indeed shows the hysteresis associated with such kinetics (as do several curves in Figures 2, 3, and 5). The hysteresis loops are wider the higher the scan rate, because the transition *into* the pit region depends on the scan rate. On the other hand, the transition *out of* the pit is virtually independent of scan speed and can be used to determine the pit width $\Delta E = E_+ - E_-$, where E_+ and E_- are the pit edges at the more positive and the more negative potential respectively. Because there is a coexistence region of several millivolts width at each edge, we have taken as pit edge the potential at which the pit capacitance joins the "normal" capacitance curve, as indicated by arrows in Figure 1 for 0.5 M guanidinium nitrate. (Quite similar results for ΔE are obtained from double potential step experiments.) As can be seen from the inset of Figure 1, the square of the pit width is a linear function of the logarithm of the guanidinium nitrate concentration.

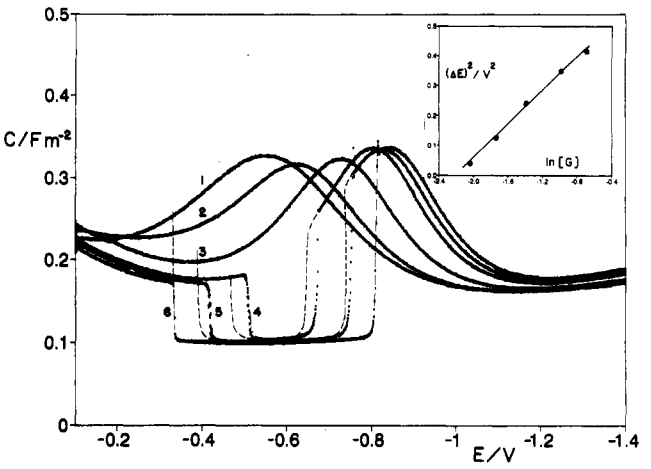

Figure 2. Same as in Figure 1, except that the measurements were made at a constant nitrate concentration of 0.5 M, with aqueous solutions containing x M of guanidinium nitrate +(0.5 − x) M of sodium nitrate, where x is (1) 0, (2) 0.006, (3) 0.034, (4) 0.130, (5) 0.176, and (6) 0.25 M. The inset shows $(\Delta E)^2$ as a function of ln [G], where [G] denotes the guanidinium concentration.

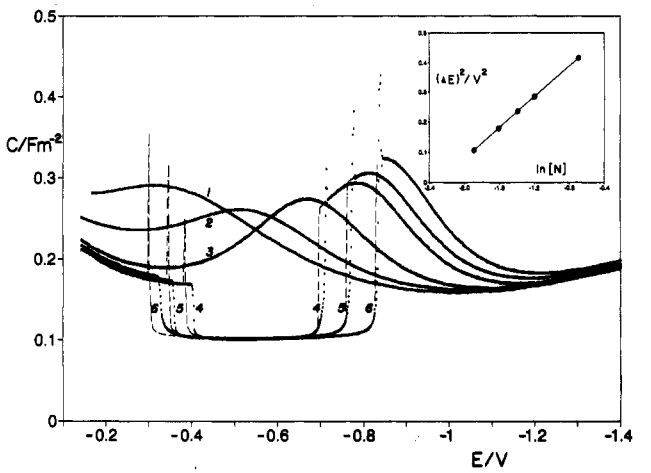

Figure 3. Same as in Figure 2, except that now the guanidinium concentration is kept constant at 0.5 M. The aqueous solutions used are x M guanidinium nitrate + (0.5 − x) M guanidinium fluoride, where x is (1) 0, (2) 0.010, (3) 0.050, (4) 0.15, (5) 0.20, and (6) 0.30 M. The inset shows $(\Delta E)^2$ as a function of ln [N] where [N] denotes the nitrate concentration.

Figure 2 shows the interfacial capacitance of a set of mixtures of guanidinium nitrate and sodium nitrate, such that the nitrate concentration is kept constant at 0.5 M. The inset shows that, under these conditions, $(\Delta E)^2$ is a linear function of the logarithm of the guanidinium concentration.

Likewise, Figure 3 illustrates the capacitive behavior of mixtures of x M guanidinium nitrate + (0.5 − x) M guanidinium fluoride, where $x \leq 0.5$. In this case, with the guanidinium concentration fixed at 0.5 M, $(\Delta E)^2$ is a linear function of the logarithm of the nitrate concentration, as can be seen in the inset of Figure 3.

The sharp "needle" peaks at the pit edges are clearly visible. The interfacial capacitance in the pit region is essentially constant, at 0.096 F m^{-2}, i.e., independent of the concentrations used, of the temperature, and (except near the pit edges) of potential. The coefficients of all linear plots mentioned so far, as determined by unweighted linear least-squares fits, are summarized in Table I.

Finally, capacitance measurements in aqueous solutions of guanidinium bromide, iodide, and thiocyanate provided no evidence for interfacial condensation in those cases, similar to the published reports for chloride[11] and perchlorate.[12] Only with sulfate did we observe formation of capacitance pits. Their study was not pursued in detail because it proved difficult to obtain

TABLE I: Values of the Parameters p and q Fitting the Linear Relation $(\Delta E)^2 = p \ln c + q$ for the Three Experimental Conditions Considered Here, viz., Simultaneous Variation of [G] and [N], Variation of [G] As [N] Is Kept Constant at 0.5 M, and Variation of [N] While [G] Is Maintained at 0.5 M[a]

c/M	p/V²	q/V²
[G] = [N]	0.54 ± 0.02	0.77 ± 0.01
[G]	0.28 ● 0.01	0.62 ± 0.01
[N]	0.26 ± 0.01	0.59 ● 0.01

[a] Here, [G] and [N] denote the bulk concentrations of guanidinium and nitrate ions respectively, in molarity. The parameters were obtained from the data shown in the insets of Figures 1–3 by nonweighted linear least-squares fitting.

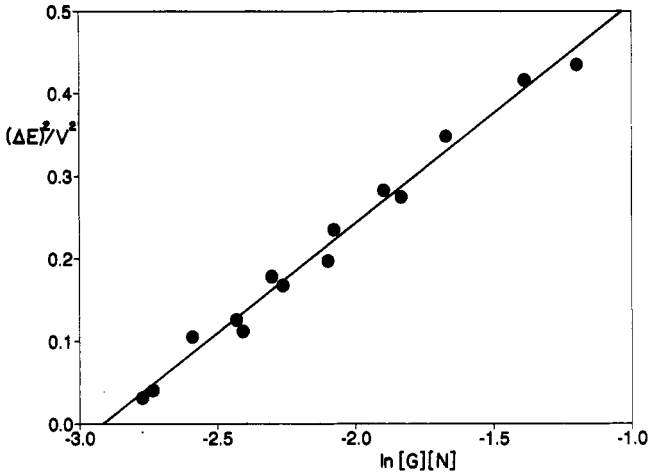

Figure 4. Composite plot of $(\Delta E)^2$ as a function of ln [G][N], where [G] denotes the guanidinium concentration, and [N] that of nitrate. The solid line represents the unweighted least-squares fit of all 15 measurements (of which two superimpose) at 5 °C, which yield $(\Delta E)^2 = (0.266 \pm 0.010) \ln [G][N] + (0.775 \pm 0.015)$, where [G] and [N] are expressed in M.

well-defined pit edges within a reasonably broad concentration range of the salt.

The linear dependencies of $(\Delta E)^2$ on the logarithm of the salt or ionic concentration, as shown in the insets to Figures 1–3, suggest that the pit region contains a one-to-one combination of guanidinium and nitrate ions, i.e., a neutral salt. The argument is based on the numerical values of the coefficients of the linear relations $(\Delta E)^2 = p \ln c + q$ as summarized in Table I. We note that the value found for p in experiments where the concentrations of both guanidinium and nitrate are varied is twice as high as that obtained when one of these concentrations is kept constant. Since, in the experiment in the absence of added electrolyte, the concentrations [G] and [N] of guanidinium and nitrate ions respectively are of course equal, we can rewrite that relation as $(\Delta E)^2 = 0.27 \ln [G][N] + 0.77$. The empirical relation for $(\Delta E)^2$ when [N] = 0.5 M can be rewritten as $(\Delta E)^2 = 0.28 \ln [G][N] + 0.81$ where $0.81 = 0.62 - 0.28 \ln 0.5$. Likewise, the variation of $(\Delta E)^2$ with [N] at constant [G] can be described by $(\Delta E)^2 = 0.26 \ln [G][N] + 0.77$ where $0.77 = 0.59 - 0.26 \ln 0.5$. Within experimental error, these three are equivalent expressions, which can be summarized as

$$(\Delta E)^2 = P \ln [G][N] + Q \qquad (1)$$

where $P = 0.266 \pm 0.010$ V² and $Q = 0.775 \pm 0.015$ V². We therefore conclude, purely on the basis of the dependence of the pit width on the guanidinium and nitrate concentrations, that the condensed film contains a one-to-one ratio of guanidinium to nitrate. Figure 4 shows the relation between $(\Delta E)^2$ and ln [G][N] for all pit widths measured at 5 °C.

A precendent for assuming the adsorption of a neutral salt can be found in the work of Murray et al. on the adsorption of lead halides at the mercury–water interface.[17-20] With guanidinium nitrate the situation is somewhat simpler, because only monovalent ions are involved. Murray et al. invoked the two-dimensional analogue of a solubility product. In the present case we have a similar situation, in that eq 1 indicates that $\Delta E^2 = 0$ when $[G][N] = \exp[-Q/P] = 0.0543$. Consequently, two-dimensional condensation of guanidinium nitrate at 5 °C is observable only when the product [G][N] exceeds 0.0543 M². This is exactly as one would expect for an interfacial solubility product.

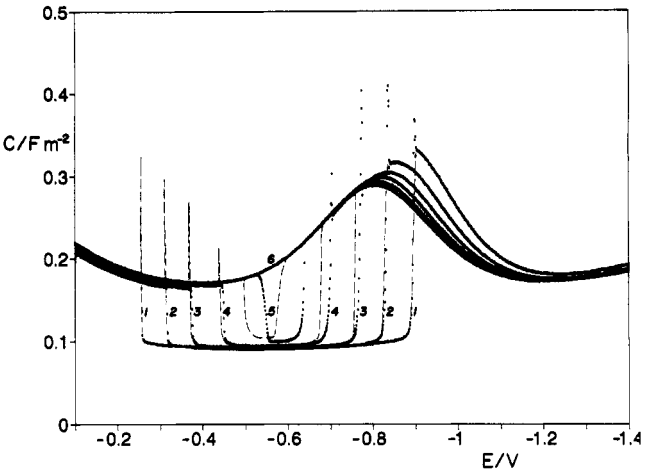

Figure 5. Same as Figure 1 except that the concentration is now fixed at 0.5 M guanidinium nitrate, while the temperature is (1) 5, (2) 11, (3) 16, (4) 20, (5) 22, and (6) 23 °C. Notice the pronounced hysteresis at 22 °C.

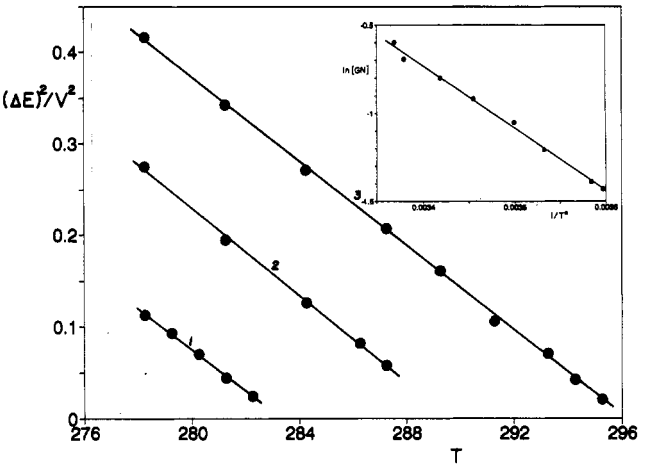

Figure 6. Square of the pit widht, $(\Delta E)^2$, as a function of absolute temperature T for aqueous guanidinium nitrate solutions of the following concentrations: 0.30 (curve 1), 0.40 (curve 2), and 0.50 M (curve 3). Lines show unweighted least-squares fits through these points. The inset shows the condensation temperature T^* as a function of guanidinium nitrate concentration.

Capacitance as a Function of Temperature

So far we have restricted our discussion to measurements at 5 °C, a constraint we will now drop. Figure 5 illustrates, for aqueous solutions of guanidinium nitrate, the dependence of the interfacial capacitance on temperature, and Figure 6 shows the resulting plots of $(\Delta E)^2$ versus absolute temperature T. These data can be extrapolated to $(\Delta E)^2 = 0$ in order to obtain a condensation temperature T^* at that particular guanidinium nitrate concentration. The resulting values of $1/T^*$ are a linear function of ln [G][N].

Similar data were obtained for mixtures of guanidinium nitrate and sodium nitrate at constant (0.5 M) nitrate concentration and for mixtures of guanidinium nitrate and guanidinium fluoride at [G] = 0.5 M (not shown). In all these cases, linear plots of $(\Delta E)^2$

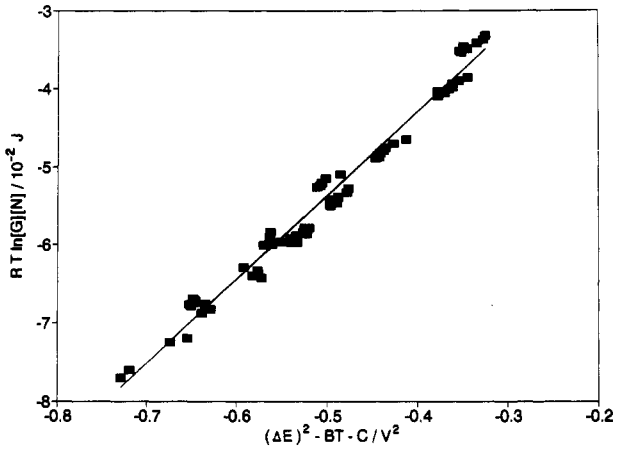

Figure 7. Composite plot of $RT \ln [G][N]$ as a function of $(\Delta E)^2 - BT - C$, where [G] denotes the guanidinium concentration, and [N] that of nitrate, in moles/liter. The vaues for B and C were taken from the least-squares analysis as $B = -0.002\ 135\ V^2\ K^{-1}$ and $C = 6.696\ V^2$. The solid line represents the unweighted least-squares fit of all 81 measurements at six different temperatures, ranging from 278.2 (5.0 °C) to 296.2 K (23.0 °C). Also shown is the straight line drawn with $A = 0.000\ 112\ 1$ mol F^{-1}.

versus T at constant [G] and [N] were obtained, and linear plots of $1/T^*$ vs ln [G][N], ln [G], or ln [N], respectively.

Formal Description

The combination of all experimental data obtained for the pit width as a function of the concentrations [G] and [N] and temperature T obeys the empirical equation

$$(\Delta E)^2 = ART \ln [G][N] + BT + C \qquad (2)$$

where A, B, and C are constants and R is the gas constant. Figure 7 displays the results for all 76 values of $(\Delta E)^2$ obtained experimentally at various values of [G], [N], and T. The solid line was calculated from a three-parameter unweighted least-squares fit as $AR = 0.000\ 932\ V^2\ K^{-1}$, $B = -0.002\ 135\ V^2\ K^{-1}$ and $C = 6.696\ V^2$.

At constant T, eq 2 reduces to eq 1 with $P = ART$ and $Q = BT + C$. At constant concentration (i.e., at a constant value of the product [G][N]), we have $(\Delta E)^2 = \{AR \ln [G][N] + B\}T + C$ and, consequently, a linear dependence of $(\Delta E)^2$ on T. Setting ΔE equal to zero then yields $AR \ln \{[G][N]\}^* + B = -C/T^*$, from which we obtain a linear relation between $\ln \{[G][N]\}^*$ and $1/T^*$. Clearly, all our experimentally established relationships are contained in eq 2.

We now briefly return to the formalism of an "interfacial solubility product". Specifically, eq 2 yields the explicit dependence of this quantity on temperature by setting ΔE equal to zero, so that

$$[G][N] = \exp\{-2(BT + C)/ART\} \qquad (3)$$

The form of eq 2 is similar to that used in connection with two-dimensional condensation of neutral organic species. In that case, an Ising or lattice gas model has often been used to describe the range of stability (in terms of concentration, temperature, and applied potential) of the compact film. For example, in the formalism of Rangarajan et al.,[21] the following relation was derived on the basis of a model of a two-dimensional two-state Ising model:

$$(\Delta E)^2 = ART \ln c + BT + C \qquad (4)$$

which merely differs from eq 2 in that only a single neutral species of concentration c was involved in the condensation process. Clearly, a complete statistical-mechanical description of the condensation of guanidinium nitrate from adsorbed guanidinium and nitrate ions would require more than a two-state model. However, the two-state model already provides a quite close approximation, and the mathematical complexity of a model involving more than two states therefore does not seem warranted by our experimental data. One might even rationalize the use of a two-state Ising model in our case by associating one state with a desolvated guanidinium–nitrate aggregate, and the other with occupancy of the site by solvent or solvated ions, but that would simply be an after-the-fact justification of the formal analogy between eqs 2 and 4.

This formal analogy might even be carried one step further. It can be shown[22] that combination of eq 4 with the usual description of electrochemical adsorption leads to a simple relation between the coefficient A in eq 4, the change $\Delta\Gamma = \Gamma_f - \Gamma_i$ in interfacial excess upon condensation, and the corresponding change $\Delta C = C_i - C_f$ in interfacial capacitance, where the subscripts i and f denote the initial and final values of Γ and C upon condensation, viz.

$$A = 8\ \Delta\Gamma/\Delta C \qquad (5)$$

The values of the integral capacitance were estimated by integration over the entire pit region, and by subsequent averaging the results obtained for the different experimental conditions used. For example, for varying [N] at constant [G] we obtained $C_i = 0.24\ F\ m^{-2}$ and $C_f = 0.096\ F\ m^{-2}$, for varying [G] at constant [N] 0.245 and 0.096 F m^{-2}, and for varying both [G] and [N] 0.24 and 0.098 F m^{-2}, respectively. With $C_i = 0.24\ F\ m^{-2}$, $C_f = 0.096\ F\ m^{-2}$, and $A = 1.12 \times 10^{-4}$ mol F^{-1}, we calculate $\Delta\Gamma = 2.0\ \mu mol\ m^{-2}$, in quite reasonable agreement with the results of Dyatkina's interfacial tension measurements, $\Gamma_i = 1.2 \pm 0.3\ \mu mol\ m^{-2}$ and $\Gamma_f = 2.9\ \mu mol\ m^{-2}$.

Comparison with Crystallographic Data

As already pointed out by Dyatkina et al.,[10] both guanidinium and nitrate ions are planar and have 3-fold symmetry. They might therefore be organized in the condensed film in a copolanar arrangement. If that is a stable arrangement, one might expect a similar ionic arrangement to exist in the crystalline state. Since the crystal structure of guanidinium nitrate apparently has not been determined so far, we have done so and here report the results.

Salient details of the single-crystal X-ray structure analysis are summarized in Tables II (with information on crystal data, data collection, structure solution and refinement), Table III (with the final atomic parameters) and Table IV (with selected interatomic distances and angles). The crystal structure is composed of near-planar layers of guanidinium nitrate ions. Each layer features a pseudotrigonal arrangement of cations and anions with the creation of a large void volume, see Figure 8. The N–H···O hydrogen bonds between the ions are 294 pm long. The layers coincide with the (202) crystal plane, relative to the *I2/m* unit cell. The layers are somewhat ruffled, with adjacent ion sites tilted by approximately 15.3° with respect to each other (see Figure 9). The large void volumes in each layer are the result of the near-hexagonal ionic arrangement in order to accommodate all hydrogen bonds. The void volumes apparently lead to the observed ruffling of the layers, attempting to fill some of those void volumes. The average interlayer separation is 307.6 pm; however, because of the tilting of the ions within the layer, and the displacement of one layer with respect to those above and below it, the closest interatomic contact between the layers is substantially larger.

The area per guanidinium–nitrate pair, calculated as the volume of the unit cell divided by the product of the interlayer spacing and the number of ion pairs per unit cell, is 0.46 nm^2. This value is noticeably smaller than the 0.57 nm^2 reported by Dyatkina et al.[10] Assuming that the two-dimensional arrangement of guanidinium nitrate at the mercury–water interface is similar to that

TABLE II: Summary of the Structure Determination

Crystal Data	
empirical formula	$CH_6N_4O_3$
color and habit	colorless plate
dimensions	0.10 mm × 0.10 mm × 0.003 mm
crystal system	monoclinic
space group	*I2/m*
unit cell dimensions	a = 750.2 ± 0.2 pm b = 731.8 ± 0.3 pm c = 1032.3 ± 0.4 pm β = 91.69 ± 0.02 pm
unit cell volume	0.5665 ± 0.0005 nm²
Z (no. of molecules/unit cell)	4
calcd density	1.432 Mg m⁻³
Data Collection	
diffractometer used	Siemens P4/RA
power used	14.4 kW
radiation	Mo Kα, λ = 71.073 pm
monochromator	highly oriented graphite crystal
2θ range	7.0–45°
temp, °C	295
reflns coll	720
independent reflns	503 (R_{int} = 2.69%)
obsd reflns	263 ($F > 4.0\ \sigma(F)$)
abs correction	none applied
Structure Analysis and Refinement	
syst used	Siemens SHELXTL PLUS (PC version)
solution method	direct (SHELXS)
refinement method	full-matrix least-squares
analysis of H atoms	riding model SHELXL, constrained isotropic U; N–H dist 90.0 pm, H–N–H angle 120°
quantity minimized	$\sum w(F_o^2 - F_c^2)^2$ for all data
weighting scheme	$w^{-1} = \sigma^2(F_o^2 + (0.0645p)^2 + 0.45p$; $p = \{\max(F_o^2,0) + 2F_c^2)/3$
weighted R index (F^2, all data) = $\sum w(F_o^2 - F_c^2)/\sum wF_o^2$	0.198
R index (F, observed data) = $\sum(\|F_o\| - \|F_c\|)/\sum\|F_o\|$	0.071

in the crystal, except for the slight ruffling, we calculate an area of 0.477 nm²/ion pair. If the difference between this number and that obtained from interfacial tension data is real, then it might reflect a slight expansion of the hydrogen-bonded network in order to accommodate a water molecule in the hole.

From our point of view, the most important aspects of this crystal structure are (a) that it shows the strong tendency of guanidinium nitrate to form planes of hydrogen-bonded ions (even at the expense of not quite filling the available space), in a structure eminently suitable for an interfacial monolayer; (b) that the area occupied in the crystal plane by a guanidinium–nitrate ion pair is smaller than but still compatible with the value determined electrochemically; (c) that such a structure would indeed represent the loss of water of hydration by both ions; and (d) that the resulting, lacelike structure has fairly large holes which, when present at the mercury–water interface, might possibly accommodate a water molecule, despite the fact that all hydrogen-bonding valencies of guanidinium and nitrate ions are clearly saturated by the structure shown in Figure 8.

We conclude that a likely ionic arrangement in the guanidinium nitrate films at the mercury–water interface is a hexagonal array of coplanar, hydrogen-bonded ions, possibly containing loose water molecules, quite different from the tight-fitting, one-dimensional ribbons of hydrogen-bonding molecules postulated earlier for condensed thymine films.[23] We assume that it is the multiple hydrogen bonding between adjacent guanidinium and nitrate ions, after they relinquish their water of hydration as postulated by Dyatkina et al.,[10] which is responsible for the formation of the condensed interfacial monolayer film.

TABLE III: Fractional Atomic Coordinates x, y, and z for Non-Hydrogen Atoms, and Equivalent Isotropic Displacement Coefficients U_{eq}[a]

	x	y	z	U_{eq}
N(1)	+0.300 19	0	+0.066 29	+0.0737
	±0.000 88		±0.000 64	±0.0021
O(1)	+0.341 56	+0.149 99	+0.121 47	+0.0961
	±0.000 58	±0.000 60	±0.000 36	±0.0019
O(2)	+0.216 57	0	−0.042 78	+0.0898
	±0.000 81		±0.000 57	±0.0022
C(1)	+0.657 37	0	+0.388 52	+0.0667
	±0.000 88		±0.000 60	±0.0020
N(2)	+0.596 39	+0.151 19	+0.343 73	+0.0883
	±0.000 54	±0.000 58	±0.000 35	±0.0017
N(3)	+0.775 77	0	+0.479 50	+0.0963
	±0.000 78		±0.000 62	±0.0023
H(2C)	+0.636 5	+0.257 2	+0.377 1	+0.096
				±0.006
H(2D)	+0.511 8	+0.150 1	+0.280 5	+0.096
				±0.006
H(3A)	+0.816 9	+0.106 5	+0.512 9	+0.096
				±0.006
H(3–B)	+0.185 9	+0.106 0	−0.081 0	+0.096
				±0.006
H(2–A)	+0.419 6	+0.146 7	+0.189 2	+0.096
				±0.006
H(2–B)	+0.314 2	+0.254 6	+0.081 6	+0.096
				±0.006

[a] At site N(1), O(1), O(2) there lies also a guanidinium ion with occupancy 1 − (0.512 ± 0.038); conversely the site C(1), N(2), N(3) can be occupied by a nitrate. The equivalent isotropic U is defined as one-third of the trace of the orthogonalized U_{ij} tensor.

TABLE IV: Bond Lengths (pm) and Bond Angles (degrees)[a]

N(1)–O(1)	127.1 ± 0.5
N(1)–O(2)	127.3 ± 0.8
C(1)–N(2)	127.9 ± 0.5
C(1)–N(3)	127.4 ± 0.8
O(1)–N(1)–O(1A)	119.5 ± 0.6
O(2)–N(1)–O(1)	120.3 ± 0.3
O(2)–N(1)–O(1A)	120.3 ± 0.3
N(2)–C(1)–N(2A)	119.8 ± 0.6
N(2)–C(1)–N(3)	120.1 ± 0.3
N(3)–C(1)–N(2A)	120.1 ± 0.3

[a] Within experimental uncertainty, all N–O and C–N distances are 127.4 pm and all angles are 120°. Because of the disorder of guanidinium and nitrate ions, the assignment of C(1) and N(1) as carbon and nitrogen, respectively, is essentially arbitrary, as it is for the assignment of O(1) and O(2), and N(2) and N(3).

Kinetics of Film Formation

In investigations of the kinetics of film formation by neutral organic compounds it is customary to start, if at all possible, from a potential where there is no or negligible adsorption. In the present case, that is not possible: at potentials positive of the pit, there will be substantial nitrate adsorption, possibly combined with some guanidinium coadsorption, analogous to effects first reported by Gouy.[24] The reverse, i.e., strong guanidinium adsorption, and possibly some nitrate coadsorption, occurs at potentials negative of the pit region, as already described by Dyatkina et al.[10] based on interfacial tension measurements.

Figure 10 shows capacitance transients following stepwise jumps from initial potentials E_0 negative of the pit region to potentials E_1 just inside the pit region. These transients have the characteristic, sigmoid shape due to nucleation and growth, as born out more quantitatively by double-logarithmic plots of the extended fractional coverage Θ_x vs time t, as shown in the inset. In constructing such Avrami plots, we have used

$$\Theta = (C_i - C)/(C_i - C_f) \tag{6}$$

$$\Theta_x = -\ln(1 - \Theta) = \ln(C_i - C_f)/(C - C_f) \tag{7}$$

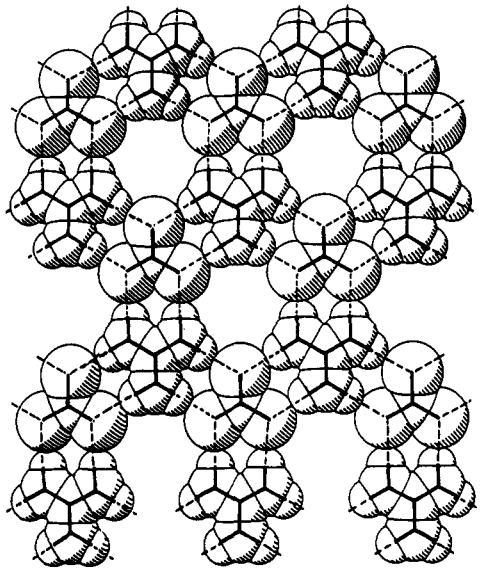

Figure 8. Arrangement of guanidinium and nitrate ions in the (202) crystal plane, shown as a space-filling model, using van der Waals radii of 0.126, 0.082, 0.130, and 0.120 nm for C, H, O, and N, respectively. The holes would be large enough to accomodate a water molecule but are unoccupied in the crystal. Overlaid is a stick diagram, which shows the chemical bonds (solid lines) and the hydrogen-bonding network (dotted lines) which holds the structure together.

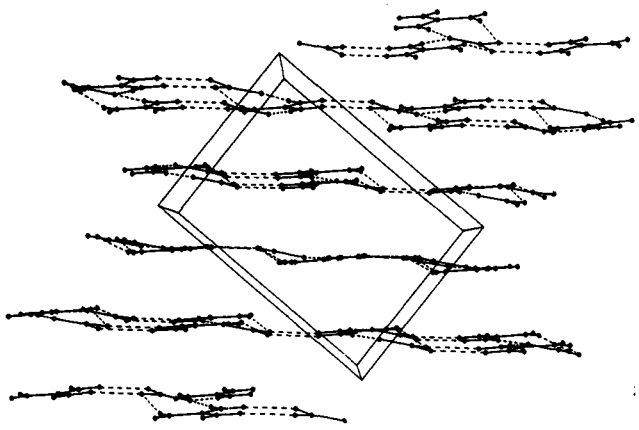

Figure 9. Perspective view of the guanidinium nitrate layers, as seen from within the central (202) plane, showing the ruffling of these planes. The outlines of the unit cell are shown for reference.

where C is the time-dependent interfacial capacitance during its transient from the initial capacitance C_i to its final value C_f. Equation 7 combines eq 6 with the Canac equation.[25] The Avrami plots yield slopes ranging from 2.9 to 3.6, with higher slopes the closer one moves to the center of the pit. Moreover, the slope depends on the initial potential: at constant final potential, the slope decreases as the initial potential is chosen closer to the pit edge, while it is independent of the time spent at the initial potential. These observations reflect the potential-dependent adsorption of guanidinium and nitrate ions outside the pit region, which apparently affects the subsequent rate of nucleation.

As illustrated in Figure 11, double potential steps can now be used to study the growth process. The potential is first stepped from its initial value E_0 to a value E_1 where nucleation occurs. It is kept there for a time so short that negligible growth takes place, whereupon the potential is changed to its final value E_2 where nucleation is too slow to be observed, yet growth of already existing nuclei continues. (The brief nucleation at E_1 is analogous to exposing a photographic film, while the subsequent stay at E_2 is akin to its development.) We find slopes of the order of 2, consistent with rate-determining, two-dimensional growth mechanism with a constant growth rate.

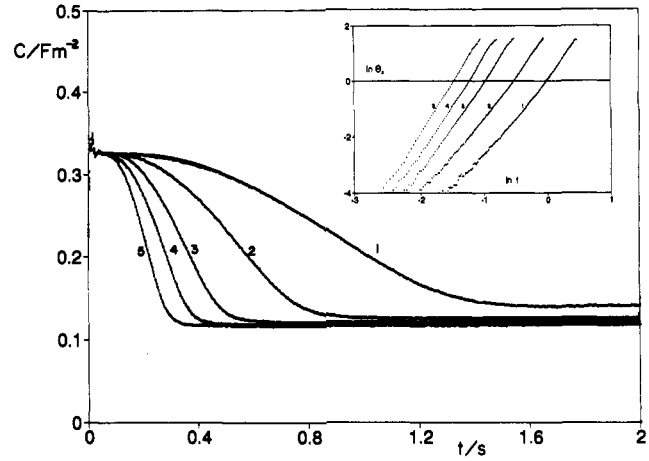

Figure 10. Capacitance transients following single potential steps from $E_0 = -1.200$ V to $E_1 = -0.805$ V (curve 1); –0.806 V (curve 2); –0.807 V (curve 3); –0.808 V (curve 4) and –0.809 V (curve 5). Solution: 0.25 M $NaNO_3$ + 0.25 M $C(NH_2)_3NO_3$, temperature 5 °C. The inset shows the corresponding Avrami plots.

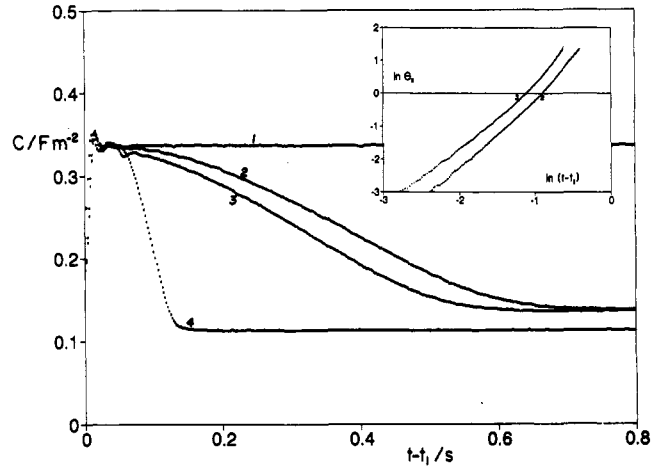

Figure 11. Capacitance transients as in Figure 10, but with double potential step measurements, starting from $E_0 = -1.200$ V with $t_0 = 5$ s, stepping first to $E_1 = -0.803$ V and, after a stay there for a time $\tau = t_1 - t_0$, to the final potential $E_2 = -0.8105$ V. The values of τ used are 0 (curve 1), 40 (curve 2), and 48 ms (curve 3). The transients shown are those following the transition $E_1 \rightarrow E_2$ at $t = t_1$. For comparison, curve 4 shows the transient following a single potential step, from $E_0 = -1.200$ V to $E_1 = -0.803$ V. The inset shows the resulting Avrami plots for curves 2 and 3.

The transients of Figure 10 can be interpreted quantitatively in terms of progressive nucleation and growth with an induction time τ:

$$\Theta_x = a(t - \tau)^3 \tag{8}$$

where a and τ are adjustable parameters. Alternatively, we can use an empirical relation with adjustable slope m,[26] which has been used to represent multistep nucleation[27]

$$\Theta_x = bt^m \tag{9}$$

where b and m are adjustable parameters. Nonlinear regression analysis of the experimental single-step transients according to eqs 8 or 9 yields reasonable fits to either (see Table V).

We also observed well-developed nucleation and growth transients with single-step and double-step experiments starting from potentials positive of the pit region, and stepping into the pit region near its positive edge. Some resulting capacitance transients starting from –0.200 V are illustrated in Figures 12 and 13. The Avrami slopes are approximately 3 and 2 for single-step and double-step experiments respectively, suggesting that a simple sequence of progressive nucleation followed by two-

TABLE V: Parameters of the Nonlinear Regression Analysis of Single Potential Step Experiments for the Transients Shown in Figure 11, Starting at E_0 = –1.200 V and Stepping to the Potential E_1 Shown in the First Column[a]

E_1/V	a/s^{-3}	τ/ms	σ	b/s^{-m}	m	σ
–0.805	142 ± 3	33 ± 1	0.011	224 ± 5	3.63 ± 0.01	0.006
–0.806	61 ± 1	32 ± 2	0.013	78 ± 2	3.49 ± 0.02	0.009
–0.807	24.5 ± 0.5	25 ± 2	0.012	26.4 ± 0.4	3.29 ± 0.02	0.009
–0.808	5.03 ± 0.06	–7 ± 2	0.010	5.19 ± 0.05	2.98 ± 0.01	0.010
–0.809	0.951 ± 0.008	15 ± 2	0.009	1.090 ± 0.003	2.86 ± 0.01	0.010

[a] Columns 2–4 show the fitting parameters to eq 8, columns 5–7 those to eq 9. The values of the standard deviation σ listed in columns 4 and 7 refer to the differences between the experimental values of θ and those calculated from eq 7 with eq 8 and 9, respectively.

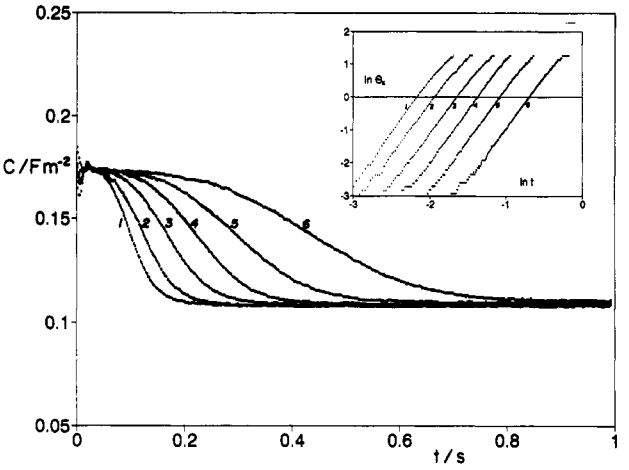

Figure 12. Capacitance transients as in Figure 10, but with E_0 = –0.200 V and E_1 = –0.332 (curve 1), –0.331 (curve 2), –0.330 (curve 3), –0.329 (curve 4), –0.328 (curve 5), and –0.327 V (curve 6). The inset shows the corresponding Avrami plots.

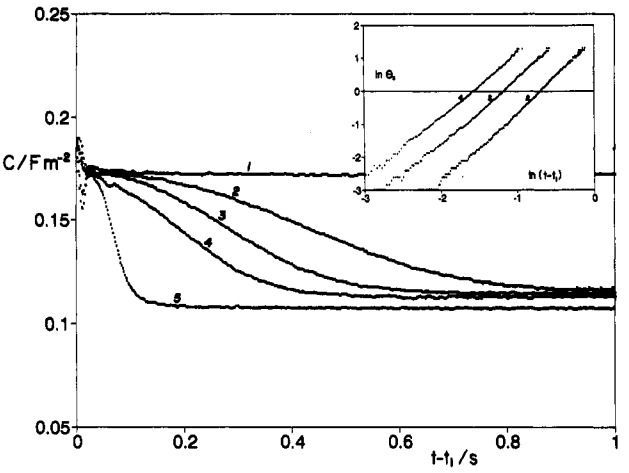

Figure 13. Capacitance transients as in Figure 11, but with E_0 = –0.200 V, E_1 = –0.331 V, and E_2 = 0.325 V. Times τ spent at E_1: 0 (curve 1), 30 (curve 2), 40 (curve 3), and 50 ms (curve 4). For comparison, curve 5 shows the capacitance transient following a single step from E_0 to E_1. The inset shows the Avrami plots for cures 2–4.

dimensional growth is responsible for these capacitance transients (see Table VI).

We already alluded to the preexisting adsorption at the potential E_0 which is the starting point of our potential step measurements, and we will now demonstrate its effect. Figure 14 shows that, at constant final potential, there is a pronounced dependence of the capacitance transients in single potential step experiments on the initial potential used. Analysis of these transients using eq 8 yielded excellent fits with exponents m equal to 2, 3, and 4 for the initial potentials –0.300, –0.200, and –0.100 V, respectively. Assuming that the growth process in all these cases (which share

TABLE VI: Parameters of the Nonlinear Regression Analysis of Single Potential Step Experiments for the Transients Shown in Figure 12, Starting at E_0 = –0.200 V and Stepping to the Potential E_1 Shown in the First Column[a]

E_1/V	a/s^{-3}	τ/ms	σ	b/s^{-m}	m	σ
–0.332	780 ± 14	5.0 ± 0.5	0.009	910 ± 44	3.13 ± 0.02	0.010
–0.331	360 ± 5	–2.0 ± 0.1	0.009	369 ± 12	3.03 ± 0.01	0.009
–0.330	150 ± 1	3.6 ± 0.5	0.007	154 ± 3	3.04 ± 0.01	0.007
–0.329	75.1 ± 0.2	13.0 ± 0.5	0.005	83.5 ± 0.7	3.19 ± 0.01	0.005
–0.328	29.3 ± 0.2	11.0 ± 0.5	0.005	30.1 ± 0.2	3.12 ± 0.01	0.005
–0.327	9.2 ± 0.1	16.0 ± 0.7	0.005	8.99 ± 0.04	3.11 ± 0.01	0.006

[a] Columns 2–4 show the fitting parameters to eq 8, columns 5–7 those to eq 9. The values of the standard deviation σ listed in columns 4 and 7 refer to the differences between the experimental values of θ and those calculated from eq 7 and eqs 8 and 9, respectively.

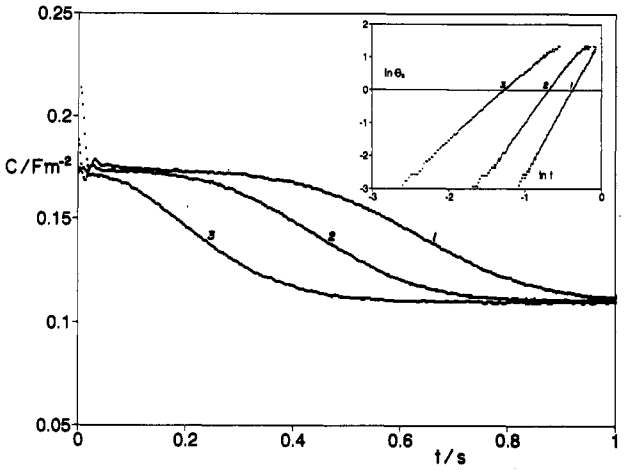

Figure 14. Capacitance transients following single potential steps as in Figure 10, but with a variable initial potential E_0 of –0.100 V (curve 1); –0.200 (curve 2) and –0.300 V (curve 3), while E_1 is fixed at –0.327 V. The corresponding Avrami plots are shown in the inset.

the same final potential; see Figure 13) remains that of two-dimensional rate-limiting growth, this result represents a gradual change from instantaneous nucleation to progressive one-step nucleation to possibly multistep nucleation,[27] especially since intermediate, noninteger Avrami slopes in the range $2 \leq m \leq 4.5$ were obtained with intermediate initial potentials. In general, the closer the initial potential is to the pit edge, the lower is the Avrami exponent m. This result reflects the existence, prior to the potential jump, of guanidinium–nitrate ion pairs and possibly aggregates thereof (which may act as prenuclei) at the mercury–solution interface.

Kinetics of Film Dissolution

When the potential is stepped from inside to outside the pit region, the film dissolves, and we can observe a corresponding capacitance transient. Such transients resemble those reported for the dissolution of tetrabutylammonium films,[8,9] including overshoot, suggesting partial diffusion control when the final potential is just outside the pit edge.[28] Interestingly, when we use a single potential step to "overfly" the pit region (e.g., by starting from –1.200 V and jumping to the area around –0.325 V), we also observe dissolution-like transients, because the limited rise time of the potentiostat used, of the order of 1–2 ms, allows enough time for the formation of a complete guanidinium nitrate film in the middle of the pit region.

Discussion

The data reported here support the earlier conclusions[10] that a film of guanidinium nitrate is adsorbed at the mercury–water interface, in which the guanidinium-to-nitrate ratio is unity. This is also similar to what we concluded from a comparison with

crystallographic data in the case of condensed thymine films.[23] The notion that a condensed film at the mercury–water interface need not contain water was first introduced by Chevalet et al. in their work on the oxygen reduction at a mercury–water interface covered with a condensed α-quinoline film, where they observed the stabilization of the superoxide radical anion O_2^-.[29]

As mentioned by Dyatkina et al.,[10] film formation of guanidinium nitrate at the mercury–water interface can be considered to be a case of expulsion of water of hydration from that interface. In this connection we quote two related examples from solid state chemistry. Bright and Garner[30] described the kinetics of dehydration of $CuSO_4 \cdot 5H_2O$ in terms of progressive nucleation and two-dimensional growth, while Garner and Southam invoked multistep nucleation for the kinetics of dehydration of $NiSO_4 \cdot 7H_2O$.[31]

It appears likely that multiple hydrogen bonding between guanidinium and nitrate ions provides the lateral, mutually attractive interaction needed for the two-dimensional condensation at the metal–solution interface. Interfacial adsorption provides the high local concentrations of guanidinium and nitrate ions (and, possibly, also the termination at the interface of a three-dimensional network of water-based hydrogen bonds surrounding these ions in solution) necessary for such an interfacial condensation, at bulk concentrations below that at which the bulk species will crystallize.

Hydrogen bonding is a fairly direction-specific interaction, and it is therefore fully compatible with the observations that, of the anions investigated so far, guanidinium ions only form condensed interfacial monolayer films with nitrate and, to some extent, with sulfate. The role of hydrogen bonding in the formation of the compact guanidinium nitrate film explains why the phenomenon is specific for nitrate and is not observed with, e.g., chloride. Again, the directional nature of hydrogen bonding is responsible, together with the need to have both proton donors and proton acceptors. Although sulfate is tetrahedral, it apparently can satisfy the hydrogen-donating tendencies of guanidinium ions with three of its four oxygens.

The role of the electrode in the formation of the compact guanidinium nitrate film is obviously to concentrate both ions and, mostly likely, to orient them. Under those conditions, the ions can form a monolayer, in which they apparently are organized as in the crystal. However, the process stops there, because the hydrogen-bonding interactions in the plane are much stronger than the interionic contacts between adjacent crystal planes, while the effect of the electrode operates only on the first layer. This is why a monolayer can form in an unsaturated solution, i.e., long before a three-dimensional crystal is stable.

The formation of guanidinium films is affected by the presence of other adsorbable ions. For example, when we use mixtures of guanidinium nitrate and guanidinium chloride instead of those of guanidinium nitrate and guanidinium fluoride shown in Figure 3, the pit width is much reduced, mostly by a shift of E_+ toward more negative potentials. This clearly reflects competition for the surface by specifically adsorbing chloride anions, which thereby tend to reduce the interfacial excess of nitrate. For example, in 0.25 M guanidinium nitrate +0.25 M guanidinium chloride we observe $E_+ = -0.385$ V and $E_- = -0.755$ V, which can be compared with the corresponding values of 0.285 and −0.770 V, respectively, in 0.25 M guanidinium nitrate +0.25 M guanidinium fluoride.

The observation that the rate of film formation following potential steps depends on the initial potential, reflects the slow buildup of critical nuclei and the strong dependence of that process on the interfacial concentrations. The effect is amplified in the present case by the opposite adsorption tendencies of cations and anions.

Finally, we note that we have so far not found any effect of the compact guanidinium nitrate film on electrode kinetics, at least on the time scale (of the order of 1–10 s) of polarogratphic experiments. We have tested the polarographic reductions of Cd(II), Tl(I), and $Co(NH_3)_6^{3+}$, as well as those of $S_2O_8^{2-}$ and $Cr_2O_7^{2-}$. As expected, the presence of guanidinium ions accelerates the peroxydisulfate reduction, but this effect already occurs at concentrations below 0.5 mM, well before a compact film can form. It is quite possible that the large holes in the ionic array of Figure 8 allow electroactive species to bypass the film as far as electron transfer is concerned.

Acknowledgment. We thank Prof. G. M. Sheldrich (Göttingen) for test versions of SHELXL and SHELXS. Financial support from NSF through Grant CHE-8921563 is gratefully acknowledged. Moreover, the single-crystal X-ray diffractometer used was purchased with financial support from NSF Grant CHE-9115394.

References and Notes

(1) de Levie, R. In *Advance in electrochemistry and electrochemical engineering*; Gerischer, H., Ed.; Wiley: New York, 1985; Vol. 13, p 1.
(2) Buess-Herman, C. In *Trends in Interfacial electrochemistry*; Silva, A. F., Ed.; Reidel: Dordrecht, 1986; p 205.
(3) de Levie, R. *Chem. Rev.* **1988**, *88*, 599.
(4) Buess-Herman, C. In *Adsorption of molecules at metal electrodes*; Lipkowski, J., Ross, P. N., Eds.; VCH: New York, 1992: p 77.
(5) Frumkin, A. N.; Damaskin, B. B. *Dokl. Akad. Nauk SSR* **1959**, *129*, 862.
(6) Lorenz, W. *Z. Elektrochem.* **1958**, *62*, 192.
(7) Wandlowski, T.; de Levie, R. *J. Electroanal. Chem.* **1992**, *329*, 103.
(8) Wandlowski, T.; de Levie, R. *J. Electroanal. Chem.* **1993**, *345*, 413.
(9) Wandlowski, T.; de Levie, R. *J. Electroanal. Chem.* **1993**, *352*, 279.
(10) Dyatkina, S. L.; Damaskin, B. B.; Vygotskaya, M. Z. *Elektrokhim.* **1980**, *16*, 996.
(11) Baugh, L. M.; Parsons, R. *J. Electroanal. Chem.* **1975**, *58*, 229.
(12) Damaskin, B. B.; Dyatkina, S. L.; Krasko, V. V. *Elektrokhim.* **1983**, *19*, 96.
(13) Sridharan, R.; de Levie, R. *J. Electroanal. Chem.* **1986**, *201*, 133.
(14) Jameson, G. B.; Wandlowski, T.; de Levie, R., unpublished results, **1992**.
(15) Curtis, R. M.; Pasternak, R. A. *Acta Crystallogr.* **1955**, *8*, 675.
(16) Payne, R. *J. Electrochem. Soc.* **1966**, *113*, 999.
(17) Murray, R. W.; Gross, D. J. *Anal. Chem.* **1966**, *38*, 392.
(18) Murray, R. W.; Gross, D. J. *Anal. Chem.* **1966**, *38*, 405.
(19) Herman, H. B.; McNeely, R. L.; Surana, P.; Elliott, C. M.; Murray, R. W. *Anal. Chem.* **1974**, *46*, 1258.
(20) Elliott, C. M.; Murray, R. W. *J. Am. Chem. Soc.* **1974**, *96*, 3321.
(21) Sridharan, R.; de Levie, R.; Rangarajan, S. K. *Chem. Phys. Lett.* **1987**, *142*, 43.
(22) Wandlowski, T., manuscript in preparation.
(23) Saffarian, M. H.; Sridharan, R.; de Levie, R. *J. Electroanal. Chem.* **1987**, *218*, 273.
(24) Gouy, G. *Ann. Chim. Phys.* **1903**, (7) *29*, 145.
(25) Canac, F. *Compt. Rend.* **1933**, *196*, 51.
(26) Retter, U. *J. Electroanal. Chem.* **1978**, *87*, 181.
(27) Wandlowski, T. *J. Electroanal. Chem.* **1990**, *293*, 219.
(28) Kurtyka, B.; Kaisheva, M.; de Levie, R. *J. Electroanal. Chem.* **1992**, *341*, 343.
(29) Chevalet, J.; Rouelle, F.; Gierst, L.; Lambert, J. P. *J. Electroanal. Chem.* **1972**, *39*, 201.
(30) Bright, N. F. H.; Garner, W. E. *J. Chem. Soc.* **1935**, 1872.
(31) Garner, W. E.; Southam, D. *J. Chem. Soc.* **1935**, 1705.